nature physics

ARTICLES

PUBLISHED ONLINE: 28 AUGUST 2017 | DOI: 10.1038/NPHYS4245

Spontaneous formation and dynamics of half-skyrmions in a chiral liquid-crystal film

Andriy Nych[1,2★†], Jun-ichi Fukuda[3,4,5★†], Uliana Ognysta[1,2], Slobodan Žumer[2,5] and Igor Muševič[2,5]

Skyrmions are coreless vortex-like excitations emerging in diverse condensed-matter systems, and real-time observation of their dynamics is still challenging. Here we report the first direct optical observation of the spontaneous formation of half-skyrmions. In a thin film of a chiral liquid crystal, depending on experimental conditions including film thickness, they form a hexagonal lattice whose lattice constant is a few hundred nanometres, or appear as isolated entities with topological defects compensating their charge. These half-skyrmions exhibit intriguing dynamical behaviour driven by thermal fluctuations. Numerical calculations of real-space images successfully corroborate the experimental observations despite the challenge because of the characteristic scale of the structures close to the optical resolution limit. A thin film of a chiral liquid crystal thus offers an intriguing platform that facilitates a direct investigation of the dynamics of topological excitations such as half-skyrmions and their manipulation with optical techniques.

Solitonic excitations arise as a result of broken symmetry of a continuous field, and they are protected topologically in the sense that they cannot be created or removed by continuous transformation of the underlying field[1,2]. Skyrme[3] introduced such a solitonic particle-like state in his nonlinear field theory of mesons that could account for the existence of fermionic baryons. Particle-like solitons of a similar kind not only find their place in particle physics but also are now known to be ubiquitous in various condensed-matter systems, such as two-dimensional electron gases exhibiting the quantum Hall effect[4–6] and spinor Bose–Einstein condensates[7,8], including superfluid He^3-A phase[9–11]. In particular, skyrmions in ferromagnets without inversion symmetry[12–16] have attracted considerable attention because of their potential for practical applications such as electron manipulation and information storage[17–20]. The name 'skyrmion' now refers in general to vortex-like excitations without singularities at their centre.

Although the original work of Skyrme[3] concerns topological excitations in three dimensions, two-dimensional (2D) skyrmions are the focus of many studies, including ours, on condensed-matter systems. 2D skyrmions can be characterized by their topological skyrmion number[21] $N=(1/4\pi)\int \mathrm{d}x\,\mathrm{d}y\,\mathbf{n}\cdot\left(\partial\mathbf{n}/\partial x\times\partial\mathbf{n}/\partial y\right)$, where $\mathbf{n}$ is a unit vector order parameter that orients in three dimensions but varies only in two dimensions (x,y). (Roughly speaking, N amounts to how many times the profile of $\mathbf{n}$ wraps the order parameter space.) Skyrmions with $|N|=1$ and $1/2$ are known as full- and half- skyrmions, respectively, in which $\mathbf{n}$ rotates by π and $\pi/2$, respectively, from the centre to its perimeter (Fig. 1a illustrates the latter).

In this work, as a possible arena for skyrmions, we focus on a chiral liquid crystal. The Frank elastic energy of a chiral liquid crystal[22] possesses a term proportional to $\mathbf{n}\cdot(\nabla\cdot\mathbf{n})$ shared by different chiral condensed-matter systems (Dzyaloshinsky–Moriya interaction in ferromagnets[12,23,24], and Rashba spin–orbit coupling in spinor Bose–Einstein condensates[25–27]) and is known to stabilize skyrmions[28]. Liquid crystals are advantageous over other condensed-matter systems in that they facilitate direct visualizations of topological structures by optical means without requiring extreme experimental conditions, because of their softness and large correlation lengths. Moreover, spontaneous distortions of the orientational order allowed by chirality lead to various non-trivial structures. A typical example is the intricate three-dimensional ordering of cholesteric blue phases (BPs), comprising a network of disclinations and so-called double-twist cylinders[29] (Supplementary Fig. 1a,b).

Indeed, the possibility of the formation of quasi-2D full skyrmions in a liquid crystal was discussed earlier by Bogdanov and co-workers[30–32], and in fact several old experimental studies have already spotted full-skyrmion-like textures in chiral liquid crystals[33,34], although they were not referred to as such. Recently Smalyukh and co-workers systematically generated isolated 2D full skyrmions[35] (and also 3D skyrmions and other particle-like topological excitations including hopfions[36–38]) by external stimuli such as focused laser beams[35–38], or relaxation from electrohydrodynamic instability[38]. Full skyrmion-like structures have also been shown to emerge experimentally in a chiral liquid crystal under geometrical confinement (for example, droplets[39] and microchannels[40]).

In contrast, there has been no experimental report on liquid crystalline half-skyrmions, although they were predicted theoretically[41]. Here we provide direct experimental evidence, together with theoretical corroborations, that a liquid crystal can exhibit half-skyrmions, both in a hexagonal regular arrangement and in an isolated manner, and show its intriguing dynamics observable by a conventional optical microscope. In contrast to the work of Smalyukh and co-workers, our half-skyrmions emerge spontaneously at a certain interval of thickness, just by sandwiching a chiral liquid crystal by two glass plates. Although a lattice of 2D half-skyrmions was predicted theoretically in other systems[12,42,43], and confirmed by neutron scattering to arise in the precursor state of a bulk cubic helimagnet[44], its real-space observation has been reported only for an atomically thin ferromagnet film with scanning tunnelling microscopy[15].

[1]Department of Molecular Photoelectronics, Institute of Physics, Nauky prospect, 46, Kyiv 03680, Ukraine. [2]Condensed Matter Department, Jožef Stefan Institute, Jamova 39, SI-1000 Ljubljana, Slovenia. [3]Department of Physics, Kyushu University, 744, Motooka, Nishi-ku, Fukuoka 819-0395, Japan. [4]National Institute of Advanced Industrial Science and Technology (AIST), 1-1-1 Umezono, Tsukuba 305-8568, Japan. [5]Faculty of Mathematics and Physics, University of Ljubljana, Jadranska 19, SI-1000 Ljubljana, Slovenia. †These authors contributed equally to this work. *e-mail: nych.andriy@gmail.com; fukuda.jun-ichi@phys.kyushu-u.ac.jp

NATURE PHYSICS DOI: 10.1038/NPHYS4245

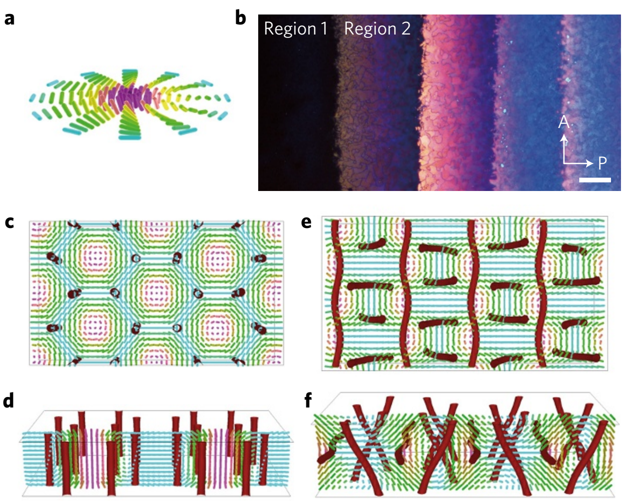

Figure 1 | Real-space structures of a thin cell of a chiral liquid crystal. **a**, Illustrations of one half-skyrmion. The colouring of short rods describing the director **n** is such that magenta and cyan represent orientational order normal and parallel to the plane, respectively. **b**, Colour image of the texture of a wedge cell under a polarizing microscope. The directions of the polarizer (P) and the analyser (A) are depicted by arrows. Cell thickness is smaller to the left. Scale bar, 50 μm. **c**,**d**, Profile of a hexagonal half-skyrmion lattice in a thinner cell whose thickness is $L = 0.597p$, where p is the natural pitch of twisted order. **e**,**f**, Structure similar to a sliced BP I in a thicker cell ($L = 0.796p$). Thick red lines are disclinations. In **c**–**f**, overall structures of 2×2 unit cells are presented. **c** and **e** present the top view of a unit cell with the director **n** at the midplane being represented by short rods whose colouring is the same as that of **a**. **d** and **f** present the perspective view of a unit cell with **n** at a vertical plane.

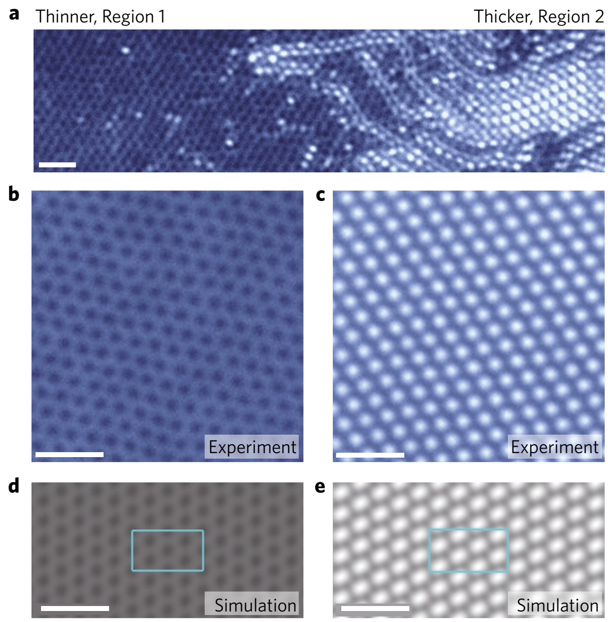

Figure 2 | Real-space observations of the half-skyrmion lattice structures and calculated real-space images. **a**, Magnified view of the transition domain between 'Region 1' (left) and 'Region 2' (right) with a boundary of complex shape. **b**,**c**, Real-space images of 'Region 1' and 'Region 2,' respectively, with a perfect periodic structure. **d**,**e**, Calculated intensity profiles of reflected light for the structures given in Fig. 1c,d and e,f, respectively. A blue rectangle denotes the region depicted in Fig. 1c,e, respectively. Scale bars, 1 μm (**a**–**c**); approximately 1 μm (**d**,**e**; see Supplementary Methods).

Real-space observation of the lattice structures

We prepared a thin film of a 1:0.65 mixture of a nematic liquid-crystal ZhK-1289 (NIOPIC) and a chiral dopant CB15 (Merck) that exhibits a thermodynamically stable blue phase known as BP I with the lattice constant $a \simeq 360$ nm (see Methods). To see the effect of the film thickness, we constructed a wedge cell with a thickness variation, using thoroughly cleaned bare cover slips imposing planar-degenerate anchoring that forces liquid-crystal molecules to be parallel to the surface, but not along any specific direction (see Methods). In Fig. 1b, we show microscopic images of the texture of the liquid crystal in the reflected light and between crossed polarizers, where the thickness increases from left to right. One can clearly identify regions with continuous colour variations and sharp colour changes between them. The latter separates regions with different structural ordering, which was observed in a previous study focusing on a thicker region of a BP wedge cell[45]. The colour variations in each region reflect the compression and dilation of the structure because of the thickness variation, leading to Bragg-like reflections with various wavelengths.

Because skyrmion-like structures were predicted to exist for a very small thickness of the BP[41], we focus our attention on the 'dark' and homogeneous left-most region in Fig. 1b (referred to as 'Region 1') and the first neighbouring and polydomain region with slightly larger thickness ('Region 2'). The border separating these two regions is located at a thickness of $L_t = 250$–260 nm. Microscope observation with a high-magnification oil-immersion objective (see Methods) immediately revealed that Region 1, although dark and apparently structureless, also has polydomain texture, as shown in Fig. 2a.

Numerically generated configurations of the liquid crystal are shown in Fig. 1c,d and e,f for different cell thicknesses L (see Supplementary Methods for technical details). For smaller L, a hexagonal lattice of half-skyrmions with disclinations of winding number $-1/2$ is predicted, as shown in Fig. 1c,d, and for larger L (Fig. 1e,f), we numerically obtain a defect structure that resembles that of the bulk BP I sliced by planes that are parallel to the [110] direction (Supplementary Fig. 1c). This orientation of the structure with the [110] plane parallel to the substrates qualitatively agrees with that of the bulk BP I ordering deduced from the Kossel diagrams (Supplementary Fig. 1d). The threshold thickness L_t at which the free energies of these two structures are the same is $L_t/a \simeq 0.6$ (see Supplementary Methods and Supplementary Fig. 2a), smaller than but close to the experimental value $(250-260)/360 \simeq 0.7$.

We now present direct real-space observations using a reflection microscope with a high numerical aperture, instead of a confocal microscope used in the previous real-space observation of bulk cholesteric BPs[46]. Figure 2a shows an enlarged part of the cell with a dark Region 1 on the left, brighter Region 2 on the right, and worm-like 'fabric fringe' structures in between.

Focusing on the dark Region 1 we immediately see a regular hexagonal lattice of dark spots with a lattice constant of 275 ± 10 nm, shown in Fig. 2b. This lattice is fully consistent with the symmetry of the hexagonal half-skyrmion lattice shown in Fig. 1c,d, whose lattice constant in real units is $\simeq$290 nm (see Supplementary Methods), close to the experimental value. The calculated microscope image of this half-skyrmion lattice (Fig. 1c,d), shown in Fig. 2d, agrees remarkably well with experiment (Fig. 2b) (see Supplementary Methods for the technical details of the calculations). The focal plane is set to the midplane of the cell, and the qualitative features of the resulting image in the calculations are insensitive to its location; see Supplementary Fig. 5a. We therefore conclude that the dark hexagonal lattice in Region 1 is a hexagonal lattice of half-skyrmions, whose centres yield dark spots. The darkness of the half-skyrmion centres is attributable to the minimal light reflection due to the small refractive-index contrast between the glass substrate and the liquid crystal with a local vertical alignment at the core of each half-skyrmion (Fig. 1c,d). On the periphery of the half-skyrmions, the director is nearly parallel to the substrates, leading to a higher refractive-index contrast and therefore a stronger reflection from these areas (Fig. 1c). Note that topological defects do not appear explicitly in either the experimental and numerical images, because of their small scale.

Note the large length-scale difference between our half-skyrmion lattice (a few hundred nanometres) and skyrmions reported by Smalyukh and co-workers[35] (tens of micrometres); in the latter, the pitch of the helical order was more than one order of magnitude larger than that of our system. See also Supplementary Discussion and phase diagrams for different pitch values in Supplementary Fig. 2a,b, for a reason why a smaller pitch is preferable for our half-skyrmion lattice.

In contrast to the dark hexagonal lattice of half-skyrmions in Region 1, bright spots arranged in a centred-rectangular lattice, with an aspect ratio of 2.1 ± 0.1, are seen in Region 2 (Fig. 2c). A calculated microscope image of this simulated structure (Fig. 1e), shown in Fig. 2e, also exhibits a regular array of bright spots (the shape of the bright spots depends on the location of the focal plane; see Supplementary Fig. 5b). Furthermore, Region 2 reflects light much more strongly than Region 1, both in the experiments (Figs 2a–c and 1b) and in the numerical calculations (Fig. 2d,e). Compared with the half-skyrmion lattice with almost uniform orientational order along the cell normal (Fig. 1d), the structure in the thicker cell exhibits strong variation of orientational order along the cell normal involving large areas of planar alignment, as is evident from Fig. 1f. Scattering of light from the inhomogeneous ordering of the liquid crystal along the normal direction is likely to contribute to a higher reflection from the Region 2 structure and local bright areas within it.

Dynamics of the skyrmion lattice

The worm-like fringes separating Regions 1 and 2 have a polygonal (zigzag) shape aligned along the local axes of the hexagonal structures of Region 1 remaining between them (Fig. 2a). At a larger thickness, the darker spaces between the fringes become brighter, and the fringes are glued together to form the structure of Region 2. Most interestingly, we observe that the half-skyrmion lattice in Region 1 and the intermediate worm-like structure are not static; instead, we clearly see vivid flickering of the spots in the half-skyrmion lattice (see Supplementary Movie 1) and very strong, worm-like fluctuations of the fabric fringe between Region 1 and Region 2 (see Supplementary Movie 2).

We first focus on the dynamics of the worm-like fluctuations of the fabric fringe intermediate region. To figure out the effect of the thermal fluctuations that are likely to drive this motion, we perform simulations of the dynamics of a chiral liquid-crystal layer, quenched from an isotropic phase. When the layer thickness is smaller than a certain threshold value, disclination lines spontaneously form almost normal to the layer and arrange themselves in a honeycomb manner, as in Fig. 1c (see also Supplementary Movie 3 and Supplementary Fig. 3). Interestingly, the simulated disclination lines are not static, but rotate occasionally in pairs or triplets as a result of the thermal fluctuations (Supplementary Movie 3). When the cell thickness is larger, horizontal disclination lines at the midplane of the cell emerge as well as those normal to the cell (Supplementary Movie 4). Recall that the numerical structure of Region 2, shown in Fig. 1e,f, contains an array of disclination lines at the midplane. These horizontal disclination lines can connect to form longer lines, or disconnect to rearrange themselves (Supplementary Movie 4 and Supplementary Fig. 4). In the course of the reorganization of the horizontal disclination lines, however, the lattice structure formed by the vertical disclination lines remains almost intact. This could explain why the motion of the fabric fringes at the boundary between Region 1 and Region 2 is restricted to follow the axes of the Region 1 structure.

We next focus on the flickering dynamics of the half-skyrmion lattice. Figure 3a shows selected movie frames of a half-skyrmion lattice taken in Region 1 (Supplementary Movies 1 and 2). One can resolve strong and frequent flickering bright spots together with the fluctuation of the background hexagonal lattice of half-skyrmions (darker spots), which again clearly manifest the nature of the fluctuations of our half-skyrmion lattice. Closer inspection reveals that the flickering bright spots appear in between the half-skyrmions in regularly ordered hexagonal domains, or are stuck to the boundaries between such domains. In the latter case, they form chains along one of the axes of the hexagonal half-skyrmion lattice.

We calculate the time evolution of a structure in a thinner cell, and the corresponding microscope images. Selected snapshots are shown in Fig. 3b. The calculated flickering behaviour is strikingly similar to that found in the experiments (Fig. 3a). The corresponding profiles of the orientational order are presented in Fig. 3c, where magenta dots correspond to the centres of the half-skyrmions, and red spots to the in-plane projection of the disclinations. All the bright spots are located at the imperfections of the hexagonally ordered half-skyrmions, particularly with diffuse red spots representing tilted disclinations. Tilted disclinations involve inhomogeneous ordering along the cell normal, and we have already shown in Figs 1f and 2e that such inhomogeneous ordering seems to scatter light, yielding bright spots. The formation of structures with locally tilted disclinations driven by thermal fluctuations is therefore likely to be responsible for a higher local reflectivity, leading to the flickering of the half-skyrmion lattice. Note also the transient nature of the local structures with tilted disclinations in Fig. 3c (see also Supplementary Fig. 3 and Supplementary Movie 3) that does not allow the persistence of isolated bright spots.

One can make a crude estimate of the fluctuation amplitude A of a vertical disclination line that yields $A/l \simeq 0.06$, where l is the distance between two neighbouring disclinations (see Supplementary Discussion). Note that A exhibits the logarithmic divergence with respect to the system size as is well known for two-dimensional systems. This estimate shows that the fluctuation of disclinations indeed exists as seen in Supplementary Movies 3 and 4, but are not strong enough to destroy the underlying hexagonal lattice of half-skyrmions (Supplementary Movie 1). Note that this estimate is based on the treatment of a honeycomb lattice of vertical disclination lines as a continuous two-dimensional elastic medium, and dislocations of the disclination lattice is not considered. Such dislocations are driven by the effective elastic force, and therefore the effect of thermal fluctuations is much more enhanced. This is why the flickering is always localized at tilted disclinations at the imperfection of the half-skyrmion lattice, and the reorganization of disclinations at the midplane, particularly curved ones (Supplementary Movie 4), is possible. We also note that the long-wavelength fluctuation of the structures (Supplementary Movie 2) is the manifestation of the presence of the Goldstone mode.

Isolated half-skyrmions

So far we have concentrated on a lattice of half-skyrmions. However, when the cell thickness was extremely small, isolated half-skyrmions were also observed in the background cholesteric phase whose pitch axis is normal to the cell. In Fig. 4a, where we used a chiral liquid crystal with larger pitch p ($\simeq$710 nm, see Methods) and the local cell thickness was $\simeq$140 nm, half-skyrmions appear as larger dark spots, while accompanying topological defects, disclination lines perpendicular to the cell, can also be seen as smaller dark spots. This identification is justified by a numerical calculation of a microscope image of an isolated half-skyrmion (Fig. 4b,c). That one half-skyrmion is accompanied by two topological defects is easily understood by a topological charge neutrality on the in-plane

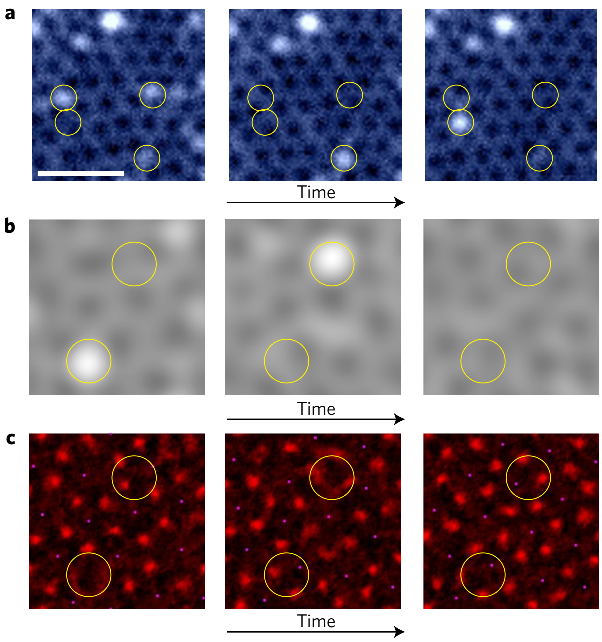

Figure 3 | Flickering of a hexagonal lattice of half-skyrmions. **a**, Microscope observation of the flickering in the hexagonal lattice of half-skyrmions. The flickering spots are highlighted by yellow circles in each panel. The time interval between neighbouring panels is 0.2 s, and the scale bar is 1 μm. **b**, Calculated time evolution of the intensity profile of monochromatic light, reflected from a hexagonal half-skyrmion lattice. The time interval between neighbouring panels is approximately 20 ms. The lateral dimension of one panel is approximately 0.92 μm. Two yellow circles highlight the flickering. **c**, Half-skyrmions (magenta dots) and disclination lines normal to the liquid-crystal layer (sharp red spots) for each panel of **b**. See Supplementary Methods for their numerical identification. Yellow circles are located at the same places as in **b**.

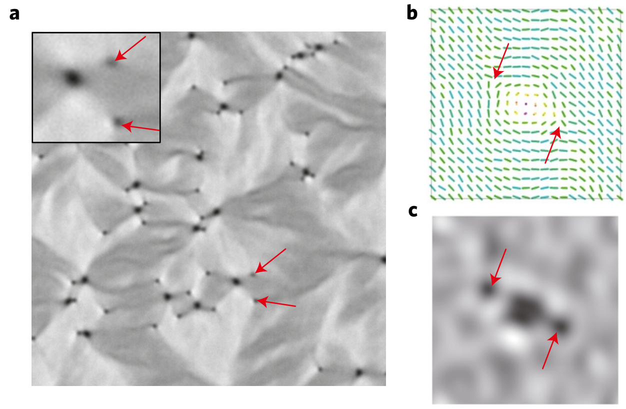

Figure 4 | Isolated half-skyrmions. a, Microscope observation of a thin cell (thickness $\simeq 140$ nm; lateral dimension of the image $= 17.87$ μm) of a chiral liquid crystal with pitch $p \simeq 710$ nm exhibiting isolated skyrmions and topological defects. The numerical aperture for illumination is $NA_{illum} \simeq 0.3$–0.4. In the inset, a magnified image of one half-skyrmion accompanied by two defects of winding number $-1/2$ is shown. **b**, Simulated isolated skyrmion (centre) carrying two topological defects. Here the orientational order at the midplane is depicted, and its colouring is the same as that of Fig. 1a. The lateral dimension is $2.546p \simeq 1.81$ μm. **c**, Corresponding calculated microscope image for $NA_{illum} = 0.3$. In each panel, topological defects with winding number $-1/2$ are highlighted by red arrows.

order (Fig. 4b). Note that two topological defects per half-skyrmion exist also in a hexagonal lattice of half-skyrmions (Fig. 1c,d). It can be safely assumed that a half-skyrmion is embedded in a liquid crystal uniformly aligned laterally (from Fig. 4b, orientational order at the midplane is practically in-plane except at the half-skyrmion centre). Then a half-skyrmion can be regarded as a topological charge of winding number $+1$ in the sense of the first homotopy group (not to be confused with the skyrmion number regarding the second homotopy group), and is compensated by two disclinations each having $-1/2$ winding number. These topological entities with charge of different sign do not annihilate because of the twist distortions of orientational order in between.

In the experiments, there are indeed around twice as many $-1/2$ disclinations as half-skyrmions, although this relation is not exact because we do not impose any condition at the lateral boundaries, and therefore the overall charge neutrality does not hold. Surprisingly, some topological defects stay away from half-skyrmions. The attractive interaction between a topological defect and a half-skyrmion could be screened, the same as the interaction between colloidal particles in a very thin cell[47]. Note also the fluctuating behaviour of topological defects and half-skyrmions (Supplementary Movie 5), similar to that of topological defects accompanying a circular inclusion in a smectic-C film[48]. This fluctuating behaviour is attributable to translational symmetry along the lateral directions and a stronger effect of thermal fluctuations in a (quasi-)2D system than in a 3D system. The fact that quasi-2D topological defects of a nematic liquid crystal can be observed as dark spots in unpolarized light[49] has been given little attention theoretically, and our experimental and numerical work sheds new light on how topological entities in a thin cell of a liquid crystal can be seen under a microscope.

Isolated half-skyrmions are preferably observed in a chiral liquid crystal with larger p (note that $p \simeq 710$ nm is larger than that used in the experiments shown in Figs 2 and 3 ($\simeq$360 nm), but still smaller than those in the previous experiments demonstrating full skyrmions[35]). This is because the background cholesteric phase necessary for the isolation of half-skyrmions is energetically more favourable for larger p (Supplementary Discussion and Supplementary Fig. 2a,b). A cholesteric phase with its helical axis normal to the cell is further stabilized by the planar-degenerate surface anchoring Nevertheless, the free energy density of half-skyrmion-like double-twist ordering is smaller than that of a cholesteric phase with a single twist in a dimension in which the director is allowed to rotate by approximately $\pi/2$ (ref. 29). This is an intuitive explanation of why half-skyrmions can exist as isolated excitations in our system.

A smaller numerical aperture for illumination (NA_{illum}) was preferable for the identification of topological defects (disclination lines normal to the cell); $NA_{illum} \simeq 0.3$–0.4 for Fig. 4a, and topological defects were almost unobservable with $NA_{illum} \simeq 1.4$ (Supplementary Fig. 6). This is just because the smaller dark spots are hidden by strong illumination due to a large NA_{illum}. Topological defects were not identified in the observation of an hexagonal half-skyrmion lattice with $p \simeq 360$ nm (Fig. 2a,b) because the characteristic length scale is smaller, and therefore large NA_{illum} was necessary.

There have been two different points of view on how to understand a lattice of skyrmions[50]: one is a 'wave' picture that regards a hexagonal skyrmion lattice as a superposition of three 'waves' of helical order[13], whereas the other views skyrmions as individual 'particles' with well-defined topological properties[12,19,28]. Our thin chiral liquid-crystal film accommodates half-skyrmions both as a regular hexagonal lattice and as isolated individual entities in a background cholesteric phase, and offers a novel and intriguing platform in which to study the nature of skyrmions.

Discussion and summary

We previously showed numerically[41] that a thin planar cell of a blue phase liquid crystal with strong normal surface anchoring can exhibit a hexagonal lattice of half-skyrmions. In this work the surface anchoring is weak planar degenerate, and therefore it is both surprising and interesting that completely different anchoring conditions give rise to almost the same structure. In the case of normal anchoring, the normal director at the centres of half-skyrmions is favoured by the confining surfaces. On the other hand, planar-degenerate anchoring stabilizes the disclination lines normal to the surfaces because the director is perpendicular to the disclination in its vicinity and therefore parallel to the surface. Hence, when the thickness of the cell is small compared with the lattice constant of bulk blue phases, structures resembling those of bulk blue phases (Fig. 1e,f and Supplementary Fig. 1c) with disclinations oblique to confining surfaces are no longer favourable, which results in the formation of a hexagonal half-skyrmion lattice.

In 2D electron gases[4–6] and chiral ferromagnets[13,14], a magnetic field of appropriate strength facilitates the formation of skyrmions. In the case of a liquid crystal, normal anchoring, although a local surface field, plays a role similar to that of a magnetic field. Planar-degenerate anchoring therefore offers a different mechanism for the stabilization of half-skyrmions through the stabilization of topological defects surrounding them. We also note that the disclination lines in our half-skyrmion lattice is of 'winding number' $-1/2$, which is allowed by the apolar nature of the director **n**. As discussed in ref. 41, in a spin system, 2D half-skyrmions cannot form a hexagonal lattice but rather a square lattice supported by -1 defects[12,15,42,43]. Surface anchoring serves as an external field other than a magnetic field, and thus provides an additional possibility for controlling the skyrmion structures.

Before concluding this work, we emphasize the challenge of obtaining optical images both in experiments and in numerical calculations, because the lattice constant of our half-skyrmion lattice is close to the resolution limit of the optical microscope ($\sim$150–200 nm). In the former, elaborate set-up and careful observations are required, and in the latter, geometrical optics is totally useless and one has to solve the full Maxwell equations for light propagation and reflection. Despite these difficulties, our combined work clearly demonstrates that optical microscopy, with careful set-up and appropriate theoretical support, can clarify the detailed structure and dynamics of materials whose characteristic lengths are close to the resolution limit. Moreover, our numerical calculations towards optical images are applicable not only to liquid crystals, and therefore will extend the possibility of optical microscopy to submicron scales and facilitate the understanding of optical properties of photonic materials, and the design of novel photonic devices.

We have presented a direct and real-time observation of the dynamics and structural transitions of spontaneously formed half-skyrmions with optical techniques. A thin film of a chiral liquid crystal thus provides an intriguing model system that facilitates the observation and manipulation of the dynamics of skyrmions and other intriguing defect structures on a scale that is much larger than, and in a manner quite different from, those for other conventional skyrmion systems. Note the remarkable simplicity of our experimental set-up (a chiral liquid crystal at room temperature sandwiched by clean glass plates without any surface treatments) and a wider possibility of controlling the experimental conditions; the pitch of the helical ordering, difficult to tune in magnetic materials, can be varied easily by changing the composition of the liquid-crystal material, and the thickness of the film is an additional relevant parameter. Optical microscopy enables the recording of the dynamics of skyrmions with frame rates high enough to observe the fluctuating behaviour, in contrast to transmission electron microscopy, which requires a few minutes to obtain one precise image in a ferromagnet[51]. Therefore, a thin film of a chiral liquid crystal can offer a platform in which to investigate fundamental properties of thermal fluctuations of topological entities. We also anticipate that the light manipulation of individual skyrmions in a liquid-crystal film is possible with the aid of photoresponsive materials[52] or optical vortices[53], similar to the direct writing and deleting of skyrmions in a thin magnetic film using a magnetic field[19], and the manipulation of hopfion-like structures on a much larger scale[35,36,54].

Methods

Methods, including statements of data availability and any associated accession codes and references, are available in the online version of this paper.

Received 12 August 2015; accepted 26 July 2017;
published online 28 August 2017

References

1. Rajaraman, R. *Solitons and Instantons. An Introduction to Solitons and Instantons in Quantum Field Theory* (North Holland, 1982).
2. Manton, N. & Sutcliffe, P. *Topological Solitons* (Cambridge Univ. Press, 2004).
3. Skyrme, T. A unified field theory of mesons and baryons. *Nucl. Phys.* **31,** 556–569 (1962).
4. Sondhi, S. L., Karlhede, A., Kivelson, S. A. & Rezayi, E. H. Skyrmions and the crossover from the integer to fractional quantum Hall effect at small Zeeman energies. *Phys. Rev. B* **47,** 16419–16426 (1993).
5. Barrett, S. E., Dabbagh, G., Pfeiffer, L. N., West, K. W. & Tycko, R. Optically pumped NMR evidence for finite-size skyrmions in GaAs quantum wells near Landau level filling $\nu = 1$. *Phys. Rev. Lett.* **74,** 5112–5115 (1995).
6. Schmeller, A., Eisenstein, J. P., Pfeiffer, L. N. & West, K. W. Evidence for skyrmions and single spin flips in the integer quantized Hall effect. *Phys. Rev. Lett.* **75,** 4290–4293 (1995).
7. Leanhardt, A. E., Shin, Y., Kielpinski, D., Pritchard, D. E. & Ketterle, W. Coreless vortex formation in a spinor Bose–Einstein condensate. *Phys. Rev. Lett.* **90,** 140403 (2003).
8. Leslie, L. S., Hansen, A., Wright, K. C., Deutsch, B. M. & Bigelow, N. P. Creation and detection of skyrmions in a Bose–Einstein condensate. *Phys. Rev. Lett.* **103,** 250401 (2009).
9. Mermin, N. D. & Ho, T.-L. Circulation and angular momentum in the *A* phase of superfluid Helium-3. *Phys. Rev. Lett.* **36,** 594–597 (1976).
10. Anderson, P. W. & Toulouse, G. Phase slippage without vortex cores: vortex textures in superfluid ^{3}He. *Phys. Rev. Lett.* **38,** 508–511 (1977).
11. Ruutu, V. M. H. *et al*. Critical velocity of vortex nucleation in rotating superfluid ^{3}He- *A*. *Phys. Rev. Lett.* **79,** 5058–5061 (1997).
12. Rößler, U., Bogdanov, A. & Pfleiderer, C. Spontaneous skyrmion ground states in magnetic metals. *Nature* **442,** 797–801 (2006).
13. Mühlbauer, S. *et al*. Skyrmion lattice in a chiral magnet. *Science* **323,** 915–919 (2009).
14. Yu, X. *et al*. Real-space observation of a two-dimensional skyrmion crystal. *Nature* **465,** 901–904 (2010).
15. Heinze, S. *et al*. Spontaneous atomic-scale magnetic skyrmion lattice in two dimensions. *Nat. Phys.* **7,** 713–718 (2011).
16. Boulle, O. *et al*. Room-temperature chiral magnetic skyrmions in ultrathin magnetic nanostructures. *Nat. Nanotech.* **11,** 449–454 (2016).
17. Fert, A., Cros, V. & Sampaio, J. Skyrmions on the track. *Nat. Nanotech.* **8,** 152–156 (2013).
18. Nagaosa, N. & Tokura, Y. Topological properties and dynamics of magnetic skyrmions. *Nat. Nanotech.* **8,** 899–911 (2013).
19. Romming, N. *et al*. Writing and deleting single magnetic skyrmions. *Science* **341,** 636–639 (2013).
20. Jiang, W. *et al*. Blowing magnetic skyrmion bubbles. *Science* **349,** 283–286 (2015).
21. Braun, H.-B. Topological effects in nanomagnetism: from superparamagnetism to chiral quantum solitons. *Adv. Phys.* **61,** 1–116 (2012).
22. de Gennes, P. G. & Prost, J. *The Physics of Liquid Crystals* 2 edn (International Series of Monographs on Physics, Oxford Univ. Press, 1995).
23. Dzyaloshinsky, I. A thermodynamic theory of "weak" ferromagnetism of antiferromagnetics. *J. Phys. Chem. Solids* **4,** 241–255 (1958).
24. Moriya, T. Anisotropic superexchange interaction and weak ferromagnetism. *Phys. Rev.* **120,** 91–98 (1960).
25. Xu, X.-Q. & Han, J. H. Emergence of chiral magnetism in spinor Bose–Einstein condensates with Rashba coupling. *Phys. Rev. Lett.* **108,** 185301 (2012).
26. Sinha, S., Nath, R. & Santos, L. Trapped two-dimensional condensates with synthetic spin–orbit coupling. *Phys. Rev. Lett.* **107,** 270401 (2011).
27. Hu, H., Ramachandhran, B., Pu, H. & Liu, X.-J. Spin–orbit coupled weakly interacting Bose–Einstein condensates in harmonic traps. *Phys. Rev. Lett.* **108,** 010402 (2012).

28. Bogdanov, A. New localized solutions of the nonlinear field equations. *JETP Lett.* **62,** 247–251 (1995).
29. Wright, D. C. & Mermin, N. D. Crystalline liquids: the blue phases. *Rev. Mod. Phys.* **61,** 385–432 (1989).
30. Bogdanov, A. & Shestakov, A. Inhomogeneous two-dimensional structures in liquid crystals. *J. Exp. Theor. Phys.* **86,** 911–923 (1998).
31. Bogdanov, A. N., Rößler, U. K. & Shestakov, A. A. Skyrmions in nematic liquid crystals. *Phys. Rev. E* **67,** 016602 (2003).
32. Leonov, A. O., Dragunov, I. E., Rößler, U. K. & Bogdanov, A. N. Theory of skyrmion states in liquid crystals. *Phys. Rev. E* **90,** 042502 (2014).
33. Kawachi, M., Kogure, O. & Kato, Y. Bubble domain texture of a liquid crystal. *Jpn. J. Appl. Phys.* **13,** 1457–1458 (1974).
34. Haas, W. E. L. & Adams, J. E. Electrically variable diffraction in spherulitic liquid crystals. *Appl. Phys. Lett.* **25,** 263–264 (1974).
35. Ackerman, P. J., Trivedi, R. P., Senyuk, B., van de Lagemaat, J. & Smalyukh, I. I. Two-dimensional skyrmions and other solitonic structures in confinement-frustrated chiral nematics. *Phys. Rev. E* **90,** 012505 (2014).
36. Smalyukh, I. I., Lansac, Y., Clark, N. A. & Trivedi, R. P. Three-dimensional structure and multistable optical switching of triple-twisted particle-like excitations in anisotropic fluids. *Nat. Mater.* **9,** 139–145 (2010).
37. Ackerman, P. J., Qi, Z. & Smalyukh, I. I. Optical generation of crystalline, quasicrystalline, and arbitrary arrays of torons in confined cholesteric liquid crystals for patterning of optical vortices in laser beams. *Phys. Rev. E* **86,** 021703 (2012).
38. Ackerman, P. J., van de Lagemaat, J. & Smalyukh, I. I. Self-assembly and electrostriction of arrays and chains of hopfion particles in chiral liquid crystals. *Nat. Commun.* **6,** 6012 (2015).
39. Posnjak, G., Čopar, S. & Muševič, I. Points, skyrmions and torons in chiral nematic droplets. *Sci. Rep.* **6,** 26361 (2016).
40. Guo, Y. *et al*. Cholesteric liquid crystals in rectangular microchannels: skyrmions and stripes. *Soft Matter* **12,** 6312–6320 (2016).
41. Fukuda, J. & Žumer, S. Quasi-two-dimensional skyrmion lattices in a chiral nematic liquid crystal. *Nat. Commun.* **2,** 246 (2011).
42. Mizushima, T., Kobayashi, N. & Machida, K. Coreless and singular vortex lattices in rotating spinor Bose–Einstein condensates. *Phys. Rev. A* **70,** 043613 (2004).
43. Su, S.-W., Liu, I.-K., Tsai, Y.-C., Liu, W. M. & Gou, S.-C. Crystallized half-skyrmions and inverted half-skyrmions in the condensation of spin-1 Bose gases with spin–orbit coupling. *Phys. Rev. A* **86,** 023601 (2012).
44. Pappas, C. *et al*. Chiral paramagnetic skyrmion-like phase in MnSi. *Phys. Rev. Lett.* **102,** 197202 (2009).
45. Blümel, T. & Stegemeyer, H. On the origin of Grandjean–Cano lines in liquid-crystalline blue phases. *Liq. Cryst.* **3,** 195–201 (1988).
46. Higashiguchi, K., Yasui, K. & Kikuchi, H. Direct observation of polymer-stabilized blue phase I structure with confocal laser scanning microscope. *J. Am. Chem. Soc.* **130,** 6326–6327 (2008).
47. Fukuda, J. & Žumer, S. Confinement effect on the interaction between colloidal particles in a nematic liquid crystal: an analytical study. *Phys. Rev. E* **79,** 041703 (2009).
48. Pettey, D., Lubensky, T. C. & Link, D. R. Topological inclusions in 2D smectic C films. *Liq. Cryst.* **25,** 579–587 (1998).
49. Oswald, P. & Pieranski, P. *Nematic and Cholesteric Liquid Crystals: Concepts and Physical Properties Illustrated by Experiments* (CRC press, 2005).
50. Rosch, A. Magnetic skyrmions: particles or waves. *Nat. Mater.* **15,** 1231–1232 (2016).
51. Yu, X. *et al*. Skyrmion flow near room temperature in an ultralow current density. *Nat. Commun.* **3,** 988 (2012).
52. Ikeda, T. & Tsutsumi, O. Optical switching and image storage by means of azobenzene liquid-crystal films. *Science* **268,** 1873–1875 (1995).
53. Nye, J. & Berry, M. Dislocations in wave trains. *Proc. R. Soc. Lond. A* **336,** 165–190 (1974).
54. Porenta, T., Ravnik, M. & Žumer, S. Complex field-stabilised nematic defect structures in Laguerre–Gaussian optical tweezers. *Soft Matter* **8,** 1865–1870 (2012).

Acknowledgements

A.N. and U.O. acknowledge partial support from NAS of Ukraine (grant 1.4B/186) and Ukrainian–Slovenian bilateral project (grants M/13-2013 and M/100-2014). J.F. thanks Slovenian Research Agency (ARRS research programme P1-0099 and project J1-2335) and the Centre of Excellence NAMASTE for generous financial support for his stay in University of Ljubljana, during which the important part of his work was carried out. J.F. is also supported by JSPS Grant-in-Aid (KAKENHI) for Scientific Research (Grant Numbers 25400437 and JP17H02947), the Cooperative Research Program of 'Network Joint Research Centre for Materials and Devices,' and the Supercomputer Center, the Institute for Solid State Physics, the University of Tokyo. I.M. and S.Ž. acknowledge support of the Slovenian Research Agency (ARRS) programme P1-0099 and grants J1-6723 and J1-7300. J.F. benefited greatly from valuable discussions with H. Kikuchi, Y. Okumura, H. Higuchi, H. Yoshida, H. Orihara, T. Ohzono and J. Kishine, and technical advice on numerical calculations by T. Miura.

Author contributions

A.N. and U.O. designed and performed the experiments. J.F. developed a framework for the calculation of microscope images, and carried out the numerical calculations. I.M. initiated the experimental work and supervised the experiments. S.Ž. supervised the theoretical work. J.F. wrote the manuscript with the input from all the other authors. All the authors discussed and analysed the results and contributed to the manuscript.

Additional information

Supplementary information is available in the online version of the paper. Reprints and permissions information is available online at www.nature.com/reprints. Publisher's note: Springer Nature remains neutral with regard to jurisdictional claims in published maps and institutional affiliations. Correspondence and requests for materials should be addressed to A.N. or J.F.

Competing financial interests

The authors declare no competing financial interests.

Methods

Materials. To obtain a chiral liquid crystal exhibiting BP I phase at temperatures slightly above room temperature, we used a mixture of a nematic liquid-crystal ZhK-1289 (NIOPIC) and a right-handed chiral dopant CB15 (Merck) at a 1:0.65 weight ratio, with the phase sequence being $N^* \xrightarrow{26\,^\circ C} \text{BP I} \xrightarrow{28.5\,^\circ C} \text{I}$. (Here N^* and I stand for a cholesteric phase and an isotropic phase, respectively). The lattice constant of BP I of this mixture, $\simeq$360 nm, was confirmed by the observation of its Kossel diagrams (Supplementary Fig. 1d). The Kossel diagrams also revealed that the [110] lattice planes of the cubic BP I ordering are parallel to the glass substrates (see Supplementary Fig. 1c for the orientation of the [110] plane).

For the observation of isolated half-skyrmions, we used a different chiral liquid-crystal material with pitch $p \simeq 710$ nm, a mixture of ZhK-1289, CB15, and a left-handed chiral dopant S811 (Merck) at a 1:0.5:0.1 weight ratio, with the phase sequence being $N^* \xrightarrow{31.5\,^\circ C} \text{I}$. The pitch was determined by microphotographs of uniform-lying-helix (ULH) textures in which the axis of twist distortions is parallel to the confining glass plates.

Experimental cells. Cells were prepared using 25×25 mm cover glass plates of 150 μm thickness, which were cleaned in an ultrasonic bath, dried and used without any further treatment. We confirmed planar-degenerate surface anchoring by filling flat cells made of the same glass plates with a nematic liquid crystal. The resulting Schlieren texture was bright with random in-plane alignment in different parts of the cells, indicating planar-degenerate anchoring. Thin wedge cells were prepared on a hot plate at 50 °C by placing a small amount of diluted water suspension of 2 μm particles along one edge of the bottom glass plate. The suspension was dilute enough to produce evenly spaced single particles along the edge acting as a cell spacer. Then a tiny (0.1–0.5 μl) drop of the liquid-crystal material was placed onto the glass plate. The drop was covered with the second plate and the plates were pressed against each other until the liquid-crystal material spread and covered the whole cell area. The cell was then placed into a programmable hot stage for fast cooling to a temperature ∼1–2 K above the BP I–I transition and subsequent slow (∼0.01 K min^{-1}) cooling into BP I phase. The small amount of the liquid-crystal material ensured strong capillary attraction between the glass plates. Therefore, no additional gluing was required and the cell was mechanically stable. Local cell thickness was determined by recording reflection spectra and fitting them using calculated model spectra with the cell thickness as a parameter. We used a spectrometer (Andor Shamrock SR-500i-D1) equipped with Andor Newton EM DU970N camera with EMCCD sensor cooled to −80 °C.

Microscopic observations. All microscopic observations were performed in reflection mode at constant temperature. To record high-resolution microscope images, we used an inverted polarizing microscope (Ti-U, Nikon) with ×100 oil-immersion objective (NA = 1.4), Nikon DS-Fi1 digital camera (pixel size 3.4×3.4 μm) and high-sensitivity Andor Neo (equipped with a Peltier-cooled sCMOS sensor) camera (pixel size 6.5×6.5 μm) combined with ×2.5 microscope magnification lens. Kossel diagrams (Supplementary Fig. 1d) were recorded with the same microscope in conoscopic observation mode from a single domain with a fully open illumination aperture diaphragm and a fully closed field diaphragm. Real-space images of the samples in Figs 2a–c and 3a were recorded with a fully open illumination aperture diaphragm and no polarizers. No dye or laser confocal set-up was used. To achieve the highest possible optical resolution of our microscope, we used a high-power light-emitting diode (LED) source (Thorlabs) with a nominal wavelength $\lambda_{\text{illum}} = 420$ nm and bandwidth (FWHM) 15 nm. The light source used for the observation of isolated half-skyrmions was a green LED with $\lambda_{\text{illum}} = 505$–$513$ nm.

Numerical calculations. The orientation profiles presented in Fig. 1 were calculated by minimizing the free energy functional of the liquid crystal in terms of a second-rank tensor $\chi_{\alpha\beta}$ describing the orientational order. We used the same calculation code as used in our previous studies[41,55] to find the equilibrium profiles of $\chi_{\alpha\beta}$ and their lattice constants that minimize the total free energy per unit area along the x–y plane in which periodic boundary conditions are imposed. The equation of motion for $\chi_{\alpha\beta}$ to obtain Supplementary Movies 3 and 4 and Supplementary Figs 3 and 4 is the same as that used in ref. 56 except that a thermal noise term satisfying the fluctuation–dissipation theorem is included in the present study. The calculations of the real-space images were carried out by solving the Maxwell equations for the electric field using plane-wave expansion along the lateral direction and finite-difference discretization along the normal direction of the cell. The reflected waves were calculated for different wavevectors of incident light, and the microscope images are the intensity profiles of reflected light at a given focal plane (the midplane of the cell for Figs 2d,e, 3b and 4c and Supplementary Fig. 6b,c). Further technical details can be found in the Supplementary Methods.

Data availability. The data that support the plots within this paper and other findings of this study are available from the corresponding authors upon reasonable request.

References

55. Fukuda, J. & Žumer, S. Cholesteric blue phases: effect of strong confinement. *Liq. Cryst.* **37,** 875–882 (2010).
56. Fukuda, J. & Žumer, S. Field-induced dynamics and structures in a cholesteric-blue-phase cell. *Phys. Rev. E* **87,** 042506 (2013).